Materials Research Bulletin 56 (2014) 65–70

Contents lists available at ScienceDirect

Materials Research Bulletin

journal homepage: www.elsevier.com/locate/matresbu

Investigation of structural and luminescent properties of Ce^{3+}/Mn^{2+} ions-doped $Ca_5(PO_4)_3F$

Lei Zhang [a], Zuoling Fu [a,*], Zhijian Wu [b], Yuan Wang [c], Xihong Fu [d], Tian Cui [a,*]

[a] State Key Laboratory of Super-hard Materials, College of Physics, Jilin University, Changchun 130012, China
[b] State Key Laboratory of Rare Earth Resources Utilization, Changchun Institute of Applied Chemistry, Chinese Academy of Sciences, Changchun 130022, China
[c] School of Chemistry and Environmental Engineering, Changchun University of Science and Technology, Changchun 130022, China
[d] Changchun Institute of Optics, Fine Mechanics and Physics, Chinese Academy of Sciences, Changchun 130033, China

ARTICLE INFO

Article history:
Received 12 October 2013
Received in revised form 9 April 2014
Accepted 16 April 2014
Available online 19 April 2014

Keywords:
A. Optical materials
B. Crystal structure
C. Luminescence
D. Optical properties

ABSTRACT

Ce^{3+}/Mn^{2+} ions-doped oxyapatite calcium fluorapatite [$Ca_5(PO_4)_3F$, FAP] has been successfully synthesized by a facile one-step hydrothermal method. The luminescent properties of Ce^{3+}- and Ce^{3+}/Mn^{2+}- activated FAP phosphors were investigated using the photoluminescence (PL) and photoluminescence excitation (PLE) spectra. The emission of Ce^{3+} was fitted by two Gaussian functions with dashed lines in wavenumber to confirm the Ce^{3+} ion simultaneously to occupy the 4f and 6h sites in $Ca_5(PO_4)_3F$ host, which was consistent with the calculated results of crystal field based on chemical bond theory. In addition, the existence of Ce^{3+} (sensitizer) can dramatically enhance the green emission of Mn^{2+} (activator) in Ce^{3+}/Mn^{2+} ions co-doped samples due to an efficient energy transfer from Ce^{3+} to Mn^{2+}. All of these results could help us understand the site assignments and optical properties of the rare earth ions doped in hexagonal $Ca_5(PO_4)_3F$.

1. Introduction

Inorganic luminescent materials/phosphors are playing a key role in the applications of lighting (e.g., fluorescent tubes and LEDs), displays (e.g., cathode tube display and field emission display), imaging (computed tomography), etc. [1–4]. The current attention on energy savings and green issues gives a boost to the development of LEDs for lighting, due to their advantages of high efficiency, compactness, long operational lifetime, and environmental friendliness [2,3]. Lanthanide ion doped phosphors are efficient luminescent materials and irreplaceable component of light emitting devices because of the abundant emission colors based on their $4f \rightarrow 5d$ transitions [5,6]. Especially, energy transfer between RE ions plays an important role in the development of color-tunable single-phased phosphors from both theoretical and practical points of view [7–9]. When the sensitizer and activator form small clusters in the host lattice, efficient energy transfer from the sensitizer to the activator takes place and it results in enhanced luminescence [10–12]. As we all know, the Ce^{3+} ion with the $4f^1$ configuration may act as a highly efficient emission center because $4f \rightarrow 5d$ transitions of the Ce^{3+} ion are allowed by the Laporte parity selection rules [7,13]. In addition, the Ce^{3+} ion is a well-known sensitizer for trivalent RE ion and transitional-metal ion luminescence, and the sensitizing effects depend strongly on the host lattices into which these ions are introduced. The transition metal ion Mn^{2+} with $3d^5$ electronic configurations can give a broad emission band in the visible range owing to the forbidden d-d transition, and the emission color of Mn^{2+} can vary from green to red depending on the field. Since the d-d transition of Mn^{2+} is forbidden and is difficult to be pumped, the emission of Mn^{2+} ions are indirectly excited by energy transfer from the host or the sensitizer.

In recent years, research on rare earth ion doped fluoride crystals has developed tremendously because of their wide applications in solar cells, laser materials, tricolor display technology, electronics, transport and information technology [14–19]. The calcium fluorapatite ($Ca_5(PO_4)_3F$, FAP) is a good host lattice for luminescence and laser materials. In the last decade, much effort has been devoted to the investigation of the luminescent properties of FAP doped with rare earth (RE) or transition metal ions. The most well-known example is Sb^{3+} and Mn^{2+}-coactivated calcium halophosphate $Ca_5(PO_4)_3$ (F, Cl): Sb^{3+}, Mn^{2+} [20,21], which has found applications in fluorescent lamps for a long time. However, there have been few systematic theoretical and experimental studies focusing on how the fluorapatite influences the photoluminescence of the rare earth ions and transition metal ions co-doping in it [22]. So it is necessary to explore the influences of the different crystal symmetry and bonding of the hosts on the luminescence performance of Ce^{3+}, Mn^{2+} ions

* Corresponding author. Tel.: +86 431 85167966; fax: +86 431 85167966.
E-mail addresses: zlfu@jlu.edu.cn (Z. Fu), cuitian@jlu.edu.cn (T. Cui).

http://dx.doi.org/10.1016/j.materresbull.2014.04.032
0025-5408/

co-doped FAP in details based on chemical bond theory. Firstly, the aim of this work has been to carry out a systematic effort to synthesize the FAP to perform the structural and luminescent properties of the Ce^{3+} and Mn^{2+} ions. In addition, we also obtained highly efficient luminescence of Mn^{2+} by doping Ce^{3+} in the FAP.

2. Experimental

2.1. Synthesis of the samples

2.1.1. Materials

All reagents were analytically pure, produced by Beijing Chemical Reagent Plant, and used without further purification. The sodium fluoride (NaF) was used as the fluoride source, rare earth nitrate were used to offer the cerium source, $Ca(NO_3)_2{\cdot}4H_2O$, $MnCl_2$ and $(NH_4)_2HPO_4$ were used as the calcium, manganese and phosphate source, respectively. Meanwhile, trisodium citrate was used as the "shape modifier".

2.1.2. Synthesis

In a typical procedure of luminescent $Ca_5(PO_4)_3F$ sample, the first mixture: 2 mmol $Ca(NO_3)_2{\cdot}4H_2O$ (0.4723 g) and 0.2 g of trisodium citrate were first dissolved in 20 mL deionized water as solution 1 with stirring to form a transparent homogeneous solution. Subsequently, the second mixture: 4 mmol of NaF (0.1680 g) and 1.67 mmol $(NH_4)_2HPO_4$ (0.2205 g) were added into 15 mL deionized water with stirring to form a transparent homogeneous solution as solution 2. After strong magnetic stirring at room temperature for 20 min, we introduced solution 2 dropwise into solution 1 with vigorous magnetic stirring at room temperature for 60 min to form an aqueous solution. Then, the resultant solution was transferred into a 60 mL Teflon autoclave. The autoclave was sealed and maintained at 180 °C for 24 h with the heating rate of 5 °C min^{-1} by cooling to the room temperature naturally. Finally, the precipitates were washed with deionized water and ethanol three times in sequence. The final product was dried at 60 °C for 12 h in the air. Then, in a typical preparing procedure of $Ca_5(PO_4)_3F$: (2 mol%) Ce^{3+}, (2 mol%) Mn^{2+} powders, the first mixture: 1.92 mmol of $Ca(NO_3)_3{\cdot}6H_2O$, 0.04 mmol of $Ce(NO_3)_3{\cdot}6H_2O$, 0.04 mmol of $MnCl_2$ and 0.2 g of trisodium citrate were first added into 20 mL of deionized water with stirring to form a transparent homogeneous solution as solution 1. The next steps were the same as the preparation of $Ca_5(PO_4)_3F$ crystals. Finally, we can obtain $Ca_5(PO_4)_3F$: (2 mol%) Ce^{3+}, (2 mol%) Mn^{2+}. Similarly, other samples were synthesized by the same process.

2.2. Characterization

X-Ray powder diffraction (XRD) measurements were performed on a Rigaku-Dmax 2500 diffractometer at a scanning rate of 15° min^{-1} in the range from 15° to 80°, with graphite-monochromatized Cu-Kα (λ = 0.15405 nm) radiation. The ultraviolet–visible photoluminescence excitation and emission spectra were recorded with a Hitachi F-7000 spectrophotometer equipped with Xe-lamp as an excitation source. The morphology of the obtained samples was investigated by field emission-scanning electron microscopy (FE-SEM, JSM-6700F, JEOL). All the measurements were performed at room temperature.

3. Results and discussions

3.1. Phase and structure

The composition and phase purity of the as-prepared powder samples were first examined by XRD. Fig. 1 shows the representative XRD patterns of FAP: $0.02Ce^{3+}$, $0.02Mn^{2+}$ sample. It is obvious

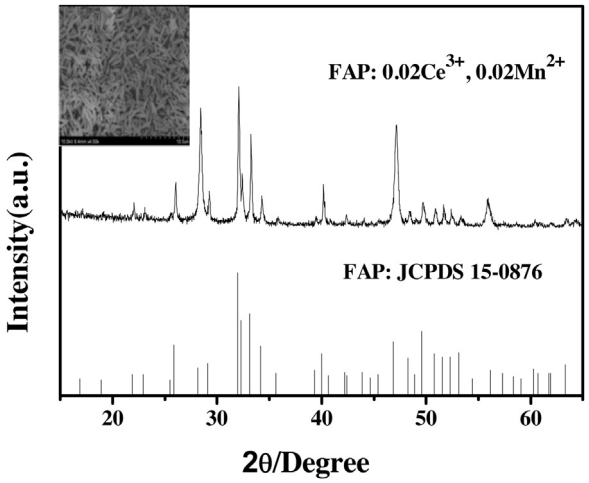

Fig. 1. XRD patterns of as-prepared FAP: $0.02Ce^{3+}$, $0.02Mn^{2+}$ sample by hydrothermal process at 180 °C for 24 h and the standard data of fluorapatite (JCPDS 15-0876). The inset is the corresponding product low-magnification FE-SEM image.

that all the diffraction peaks of the sample can be readily indexed to pure hexagonal phase of calcium fluorapatite (with space group: $P6_3/m$, no. 176) according to the JCPDS files no. 15-0876. No additional peaks of other phases have been found, indicating that the Ce^{3+} and Mn^{2+} ions have been effectively built into the host lattice. The FE-SEM image (inset in Fig. 1 at the top left corner) shows that the product is composed of well dispersed microrods with lengths around 2–3 μm and diameters around 500 nm, respectively. Furthermore, Fig. 2(a) and (b) display the unit cell representation of $Ca_5(PO_4)_3F$. This structure has two cationic Ca^{2+} sites [23,24]. 40% of the Ca^{2+} ions are denoted as Ca(I) and are at the Wyckoff 4f positions, while the other 60% are denoted as Ca(II) and are at the Wyckoff 6h positions. Ca(I) has C_3 point symmetry and is surrounded by nine oxygen anions (Fig. 2(c)). Ca(II) has C_s point symmetry and is surrounded by six oxygen anions plus one F^- anion (Fig. 2(d)). From the consideration of the ionic radius and the charge, the Ce^{3+} (the effective ionic radii for CN = 7 is 1.07 Å and CN = 9 is 1.196 Å) and Mn^{2+} (the effective ionic radii for CN = 7 is 0.9 Å) ions are expected to substitute the Ca^{2+} (the effective ionic radii for CN = 7 is 1.06 Å and CN = 9 is 1.18 Å) sites in the $Ca_5(PO_4)_3F$ crystal structure.

3.2. Photoluminescence properties

3.2.1. Optical properties of $Ca_5(PO_4)_3F$: Ce^{3+}

As we all know, the Ce^{3+} ion with the $4f^1$ configuration may act as a highly efficient emission center because 4f → 5d transitions of the Ce^{3+} ion are allowed. The excitation and emission spectra of FAP: $0.02Ce^{3+}$ sample are presented in Fig. 3. The emission spectrum (red line, right) of FAP: $0.02Ce^{3+}$ exhibited a broad band that extended from 355 to 390 nm with a maximum at about 365 nm when excited by 291 nm UV light, which was due to the 5d → 4f transition of Ce^{3+}. The corresponding excitation spectrum (black line, left) included a strong broad band from 255 to 315 nm (center, 291 nm). In addition, it can be observed that the Ce^{3+} singly doped sample exhibited a broad asymmetric emission band centering at 365 nm, which can be resolved by a Gaussian fit into two emission bands with the peak at 366 nm and 384 nm (the green and the pink lines are shown in Fig. 3) respectively. It is well known that the Ce^{3+} emission should be composed of a double band in view of the splitting of its ground state. The energy difference of this splitting between $^2F_{7/2}$ and $^2F_{5/2}$ of Ce^{3+} is about 2000 cm^{-1}. However, the energy difference between 366 nm

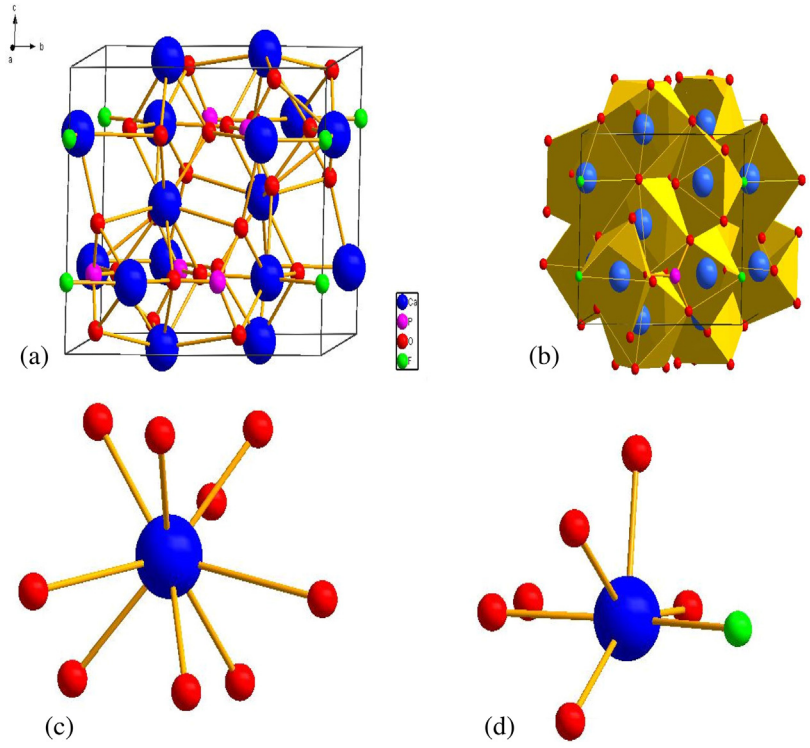

Fig. 2. (a) and (b) Unit cell representation of the crystal structure of $Ca_5(PO_4)_3F$. Blue, magenta, red, and green spheres represent Ca, P, O, and F atoms, respectively. Calcium sites 4f and 6h are described by (c) and (d), respectively.

(27322 cm^{-1}) and 384 nm (26,041 cm^{-1}) is about 1280 cm^{-1}, which is far from 2000 cm^{-1}. Therefore, these two emission bands cannot be ascribed to the ground-state splitting of the single Ce^{3+} emission center. Naturally, we can deduce that there are two types of Ce^{3+} luminescent centers in FAP. This is related to the crystal structure of FAP, which provides two different sites for the cations in it, the 4f (C_3) site and 6h (C_s) site. According to a previous report [25], the 4f site with nine-coordination needs large cations for its space, on the other hand the 6h site with seven coordination is favorable for high charge cations due to the fact that it has a O(4) ion to coordinate. The Ce^{3+} has a larger ionic radius (1.196 Å for CN = 9) and higher charge (+3), which are favorable for 4f site and 6h site, respectively. Therefore, the asymmetrical emission band (365 nm)

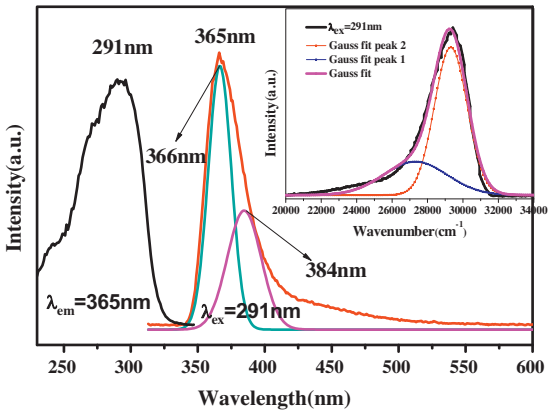

Fig. 3. Typical photoluminescence excitation and emission spectra of $Ca_5(PO_4)_3F$: $0.02Ce^{3+}$. Also, the emission of Ce^{3+} is fitted by two Gaussian functions dashed lines in wavenumber, the corresponding wavenumbers are centered at 27,322 cm^{-1} with a width of 2375 cm^{-1} for Ce^{3+} (I) band and at 26,041 cm^{-1} with a width of 4857 cm^{-1} for Ce^{3+} (II) band in the top right corner of the figure, respectively.

could originate from Ce^{3+} (4f) and Ce^{3+} (6h) luminescent sites [26–28]. Generally, it should be realized that the position of the emitting level of Ce^{3+} is determined by two factors [32–34]: (i) the position of the center of gravity of the 5d level, which will be at lower energy if the covalency increases, and (ii) the width of the crystal field splitting of the 5d level (the lower the position of the lowest crystal field component, the more the first absorption band and the emission band will move to lower energy). For the first factor, we calculated bond lengths and bond covalency of Ca—O and Ca—F in FAP based on chemical bond theory shown in Table 1, and the calculated average values of bond lengths and covalency were listed, too. We get the value of the bond covalency of Ce^{3+} (4f) and Ce^{3+} (6h), that is 0.048 for CN = 9(4f) and 0.101 for CN = 7(6h) respectively. That it is, the covalency of the Ce^{3+} (6h) is larger than Ce^{3+} (4f). For this reason, the position of the center of gravity of the 5d level in Ce^{3+} (6h) is lower than that of Ce^{3+} (4f). For the second factor, the width of the crystal field splitting of the 5d level is determined by the influence of the crystal environment. For cubic crystal field, $10D_q$ is usually expressed as the energy difference between the centers of gravity of the high-energy band and low-energy band. Although 5d orbit will split into more components when the rare earth ions are in a lower symmetry site, the magnitudes of $10D_q$ split can still be obtained based on group theory. According to the previous reports [31,32], a new parameter can be introduced, which is the combination of the four parameters [32].

$$K_e = \frac{E_h Q f_i^2}{N} \quad (1)$$

E_h is the homopolar part of average energy gap, N is the coordination number of central ion, Q is the charge of neighboring anion, and f_i is the bond ionicity between the central ion to its nearest neighboring anion. We will call K_e the environment factor according to the letter [32,33], which is crucial in determining the

Table 1
The bond length (Å) of Ca—O and Ca—F in FAP at room temperature in 4f and 6h sites. Also the average bond length, the covalency, $10Dq$ and E_h in 4f and 6h sites are presented.

	Bond type	Bond length (Å)	$\overline{d}$(Å)	f_c	$10D_q$ (cm^{-1})	E_h
4f	Ca1—O1	2.3946	2.55	0.048	20910	4.5605
(C_3 CN = 9)	Ca1—O1	2.3943				4.5605
	Ca1—O1	2.3940				4.5605
	Ca1—O2	2.4502				4.3082
	Ca1—O2	2.4497				4.3082
	Ca1—O2	2.4496				4.3082
	Ca1—O3	2.8064				3.076
	Ca1—O3	2.8055				3.076
	Ca1—O3	2.8062				3.076
6h	Ca2—O1	2.6831	2.43	0.101	57805	3.437
(C_S CN = 7)	Ca2—O2	2.3707				4.6715
	Ca2—O3	2.4840				4.4607
	Ca2—O3	2.4840				4.4607
	Ca2—O3	2.3472				4.4607
	Ca2—O3	2.3472				4.4607
	Ca2—F1	2.2944				5.0685

magnitudes of $10D_q$ split. The above parameter N can be determined from the crystallographic data [14–16]. In addition, there is a linear relation between $10D_q$ splitting and K_e. The fitted Eq. (2) is

$$\Delta E(Ce^{3+}) = 10D_q = 3.27 + 14.34K_e \quad (2)$$

ΔE is the energy difference of the two energy levels [29–31]. For $Ca_5(PO_4)_3F$ host, when N is 9, $f_i = 0.952$, $Q = 1$ and $E = 4.5605$ (Ca1—O1), 4.3082 (Ca1—O2), 3.076 (Ca1—O3) respectively. Meantime, when N is 7, $f_i = 0.899$, $Q = 2$ (Ca—O), 1.5 (Ca—F) and $E_h = 3.437$ (Ca2—O1), 4.6715 (Ca2—O2), 4.4607 (Ca3—O3) and 5.0685 (Ca—F) respectively. Finally, we can get the accurate numerical $10D_q$ of $Ca_5(PO_4)_3F$ and infer the splitting situation in different crystal lattice environment. It can be seen from Table 1 that $10D_q$ splitting in Ce^{3+} (6h) is 57805 cm^{-1}, whereas in Ce^{3+} (4f) the $10D_q$ splitting is 20910 cm^{-1}. Therefore, the width of the crystal field splitting of Ce^{3+} (6h) is bigger than the Ce^{3+} (4f). Fig. 4 shows the position of the center of gravity and the different energy splitting situations in Ce^{3+} (6h) and Ce^{3+} (4f) crystal field environment graphically. It can be seen that the position of the center of gravity of the Ce^{3+} (6h) is lower and the width of the crystal field splitting in Ce^{3+} (6h) is larger simultaneously. In conclusion, we can assign the lower-energy emission band (384 nm, 26041 cm^{-1}) to Ce^{3+} (6h, 27322 cm^{-1}) and the higher-energy emission band (366 nm) to Ce^{3+} (4f). The experimental results are consistent with the theoretical calculation results. Furthermore, it also illustrates that the different crystal symmetry and bonding of the hosts have an important influence on the luminescence performance of rare earth ions.

3.2.2. Luminescence of $Ca_5(PO_4)_3F$: Ce^{3+}, Mn^{2+}

The Ce^{3+} ion is a well-known sensitizer for trivalent RE^{3+} ion and transitional-metal ion luminescence, and the sensitizing effects depend strongly on the host lattices into which these ions are introduced. The Mn^{2+} ion with $3d^5$ electronic configuration generally shows a broad emission band whose position depends strongly on the host lattices. If the crystal field around Mn^{2+} is weak, the splitting of the excited d energy levels will be small, resulting in Mn^{2+} emission with higher energy.

Fig. 5 shows the PLE and PL spectra of the FAP: $0.02Ce^{3+}$, $0.02Mn^{2+}$. As shown in Fig. 5, the emission spectrum of the FAP: $0.02Ce^{3+}$, $0.02Mn^{2+}$ sample displays a multicolor emission when the sample is excited by 291 nm UV light, which consists of an ultraviolet emission centered at 365 nm, a blue emission band ranging from 355 nm to 390 nm and a yellow emission centered at 561 nm from 530 to 600 nm. The luminescence of Ce^{3+} has been explained explicitly, so this part aims for explaining the luminescence of Mn^{2+} and the energy transfer between Ce^{3+} and Mn^{2+} in FAP. While Mn^{2+} ions are doped singly in the FAP, we cannot detect the luminescence of Mn^{2+}. Only when Ce^{3+} and Mn^{2+} ions are co-doped in it, can we observe the luminescence of Ce^{3+} and Mn^{2+} concurrently. In this system, Ce^{3+} ions can strongly absorb UV light

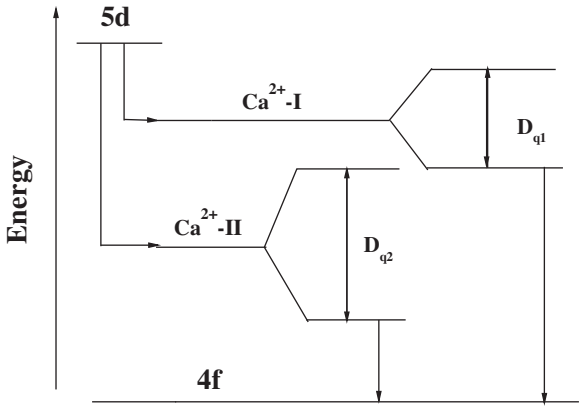

Fig. 4. A schematic energy splitting diagram of the Ce^{3+} in Ca^{2+}-I (CN = 9) and Ca^{2+}-II (CN = 7) in FAP crystals structure.

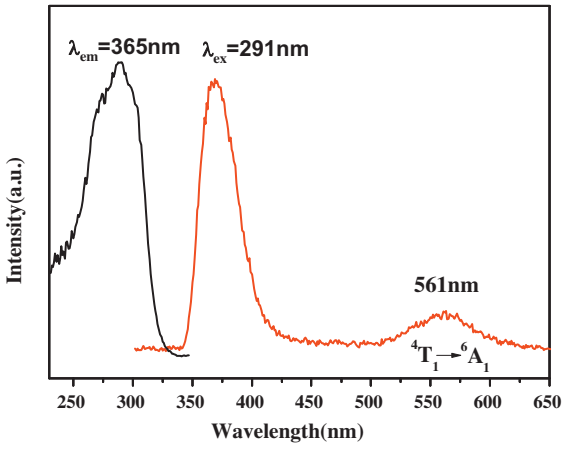

Fig. 5. Respective photoluminescence excitation and emission spectra of the $Ca_5(PO_4)_3F$: $0.02Ce^{3+}$, $0.005Mn^{2+}$ sample ($\lambda_{em} = 365$ nm; $\lambda_{ex} = 291$ nm).

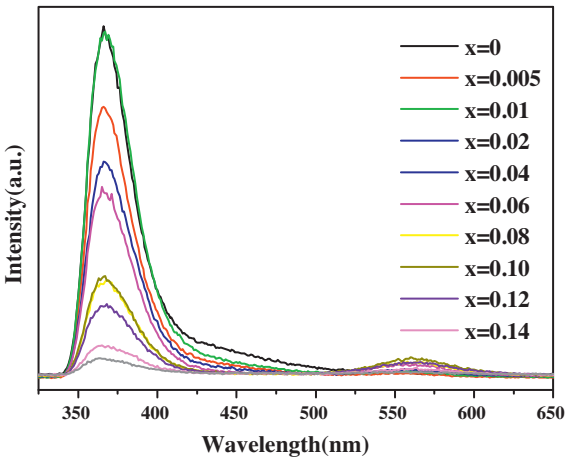

Fig. 6. The photoluminescence emission spectra of the FAP: $0.02Ce^{3+}$, xMn^{2+} with different Mn^{2+} concentrations (x = 0–0.14).

from the ground state ($^2F_{5/2}$) to the excited state and then efficiently transfer the energy to the $^4T_1$ level of Mn^{2+} ions; subsequently, the $^4T_1$ level gives its characteristic transitions and continues to transfer the energy to the $^6A_1$ level via cross-relaxation [35,36].

To investigate the energy transfer from Ce^{3+} to Mn^{2+}, a series of samples with different concentrations of Mn^{2+} ions have been prepared. As revealed in Fig. 6, the emission intensity of Ce^{3+} decreases with the increasing Mn^{2+} concentration, while the emission intensity of Mn^{2+} first increases with an increase of its concentration (x), reaching a maximum value at x = 0.08, and then decreases with a further increase (x) due to the concentration quenching effect. All of these results can validate the efficient energy transfer from Ce^{3+} to Mn^{2+}. Fig. 7(a) exhibits the tendency of this variation clearly. The energy transfer efficiency (η_T) from the Ce^{3+} to Mn^{2+} ions in $Ca_5(PO_4)_3F$: $0.02Ce^{3+}$, xMn^{2+} is calculated using the formula (3) [32]:

$$\eta_T = 1 - \frac{I_S}{I_{S0}} \quad (3)$$

where η_T is the energy transfer efficiency, I_{so} and I_s are the luminescence intensity of a sensitizer (Ce^{3+}) in the absence and presence of an activator (Mn^{2+}) respectively. The η_T value of

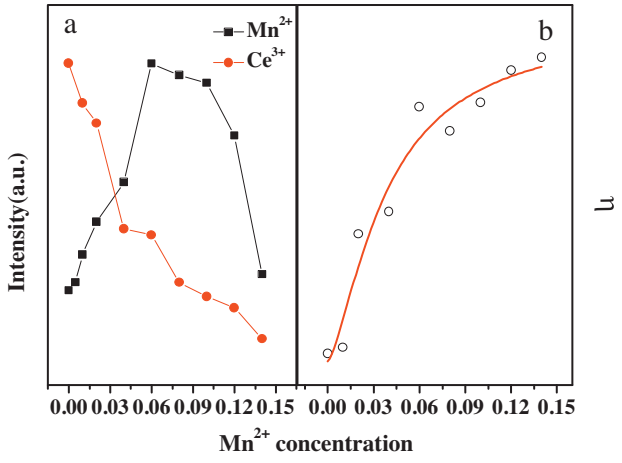

Fig. 7. (a) Dependence of the relative emission intensity of Ce^{3+} and Mn^{2+} for FAP phosphors; (b) The energy transfer efficiency (η_T) from Ce^{3+} to Mn^{2+} in FAP: $0.02Ce^{3+}$, xMn^{2+}(0–0.14) samples (λ_{ex} = 291 nm).

FAP: $0.02Ce^{3+}$, xMn^{2+} could be obtained as a function of x presented in Fig. 7(b). Also, it reveals that the energy transfer would be very effective when using 291 nm UV as the excitation wavelength with the increase of Mn^{2+} concentration. Other experiments are underway, we expect that it can realize the color tunable emission of rare earth ions in FAP by the energy transfer.

4. Conclusions

In conclusion, Ce^{3+}/Mn^{2+}-activated FAP oxyapatite structured phosphors have been prepared via hydrothermal reaction. The structural and luminescent properties of FAP: Ce^{3+} and FAP: Ce^{3+}, Mn^{2+} were investigated in details by the spectral measurement and theoretical calculation. The emission of Ce^{3+} was fitted by two Gaussian functions dashed lines in wavenumber to further confirm the Ce^{3+} ion simultaneously to occupy the 4f and 6h sites in $Ca_5(PO_4)_3F$ host. In addition, the results revealed that the existence of Ce^{3+} (sensitizer) can dramatically enhance green emission of Mn^{2+} (activator) in co-doped samples due to an efficient energy transfer from Ce^{3+} to Mn^{2+}.

Acknowledgments

This work was supported by the National Science Foundation of China (no. 11004081), partially sponsored by China Postdoctoral Science Foundation, supported by the Science and Technology Development Planning Project of Jilin Province (20130522173JH) and by the Chunmiao Talents of Jilin Province.

References

[1] G. Wakefield, E. Holland, P.J. Dobson, J.L. Hutchison, Advanced Materials 13 (2001) 1557.
[2] A.A. Setlur, W.J. Heward, Y. Gao, A.M. Srivastava, R.G. Chandran, R.G.M.V. Shankar, Chemistry of Materials 18 (2006) 3314.
[3] Y.Q. Li, A.C.A. Delsing, G. de With, H.T. Hintzen, Chemistry of Materials 17 (2005) 3242.
[4] Z. Li, J.C. Barnes, A. Bosoy, J.F. Stoddart, J.I. Zink, Chemical Society Reviews 41 (2012) 2590.
[5] Y. Wei, F.Q. Lu, X.R. Zhang, D.P. Chen, Journal of Alloys and Compounds 427 (2007) 333.
[6] C. Feldmann, T. Justel, C.R. Ronda, P.J. Schmidt, Advanced Functional Materials 13 (2003) 511.
[7] N. Guo, Y. Song, H. You, G. Jia, M. Yang, K. Liu, Y. Zheng, Y. Huang, European Journal of Inorganic Chemistry 29 (2010) 4636.
[8] C.H. Huang, T.M. Chen, W.R. Liu, Y.C. Chiu, Y.T. Yeh, S.M. Jan, ACS Applied Materials and Interfaces 2 (2010) 259.
[9] A. Suchocki, B. Koziarska, A. Brenie, C. Pedrini, G. Boulon, Journal of Alloys and Compounds 225 (1995) 559.
[10] V. Singh, M. Tiwari, T.K.G. Rao, S.J. Dhoble, Bulletin of Materials Science 28 (2005) 31.
[11] B. Wei, Z. lin, G. Wang, Journal of Crystal Growth 295 (2006) 241.
[12] A. Nag, T.R.N. Kutty, Chemical Physics 91 (2005) 524.
[13] G. Blasse, A.J. Bril, Chemical Physics 47 (1967) 5139.
[14] P. Solarz, G. Dominiak-Dzik, W. Rvba-Romanowski, Journal of Alloys and Compounds 362 (2004) 61.
[15] C.Y. Xiang, W. Koo, F. So, H. Sasabe, J. Kido, Light: Science and Applications 2 (2013) e74.
[16] V. Sivakumar, U.V. Varadaraju, Journal of the Electrochemical Society 156 (2009) 179.
[17] E. Matioli, S. Brinkley, K.M. Kelchner, Y.L. Hu, S. Nakamura, S. DenBaars, J. Speck, C. Weisbuch, Light: Science and Applications 1 (2012) e22.
[18] H.S. Jang, K. Woo, K. Lim, Optics Express 20 (2012) 17107.
[19] R. Scheps, Progress in Quantum Electronics 20 (1996) 271.
[20] G. Blasse, B.C. Grabmaier, Luminescent Materials, Springer-Verlag, Berlin, 1994.
[21] S. Shionoga, W.M. Yen, Phosphor Handbook, CRC Press, Boston, 1999.
[22] D.Q. Chen, Y.L. Yu, F. Huang, P. Huang, A.P. Yang, Y.S. Wang, Journal of the American Chemical Society 132 (2010) 9976.
[23] Y.W. Lunt, M.G. Zhao, Z.Q. Lin, Journal of Physics C: Solid State Physics 18 (1985) 1857.
[24] M.M. Shang, D.L. Geng, D.M. Yang, X.J. Kang, Y. Zhang, J. Lin, Inorganic Chemistry 52 (2013) 3102.
[25] J. Lin, Q. Su, Materials Chemistry and Physics 38 (1994) 98.
[26] Q. Zeng, H.B. Liang, G.B. Zhang, M.D.N. Birowosuto, Z.F. Tian, H.H. Lin, Y.B. Fu, P. Dorenbos, Q. Su, Journal of Physics: Condensed Matter 18 (2006) 9549.

[27] Y.Q. Li, N. Hirosaki, R.J. Xie, T. Takeda, M. Mitomo, Chemistry of Materials 20 (2008) 6704.
[28] G.G. Li, Y. Zhang, D.L. Geng, M.M. Shang, C. Peng, Z.Y. Cheng, J. Lin, Applied Materials and Interfaces 4 (2012) 296.
[29] G. Blasse, A. Bril, Journal of Chemical Physics 47 (1967) 5139.
[30] G.G. Li, D.L. Geng, M.M. Shang, C. Peng, Z.Y. Cheng, J. Lin, Journal of Materials Chemistry 21 (2011) 13334.
[31] J. Lin, Q. Su, Journal of Materials Chemistry 5 (1995) 1151.
[32] C.H. Huang, T.W. Kuo, T.M. Chen, ACS Applied Materials and Interfaces 2 (2010) 1395.
[33] L.A. Riseberg, H.W. Moos, Physical Review Letters 74 (1968) 429.
[34] J.S. Shi, Z.J. Wu, S. Zhou, S.Y. Zhang, Chemical Physics Letters 380 (2003) 245.
[35] C.M. Zhang, S.S. Huang, D.M. Yang, X.J. Kang, M.M. Shang, C. Peng, J. Lin, Journal of Materials Chemistry 20 (2010) 6674.
[36] M. Li, Y. Sheng, Spectroscopy Spectral Analysis 28 (2008) 2352.